

# Optimized Dynamic Acousto-elasticity Applied to Fatigue Damage and Stress Corrosion Cracking

Sylvain Hauptert · Jacques Rivière · Brian Anderson · Yoshikazu Ohara · T. J. Ulrich · Paul Johnson

Received: 31 October 2013 / Accepted: 23 January 2014 / Published online: 8 February 2014  
© Springer Science+Business Media New York 2014

**Abstract** The dynamic acousto-elasticity (DAE) technique uniquely provides the elastic (speed of sound and attenuation) behavior over a dynamic strain cycle. This technique has been applied successfully to highly nonlinear materials such as rock samples, where nonlinear elastic sources are present throughout the material. DAE has shown different nonlinear elastic behavior in tension and compression as well as early-time memory effects (i.e. fast and slow dynamics) that cannot be observed with conventional dynamic techniques (e.g. resonance or wave mixing measurements). The main objective of the present study is to evaluate if the DAE technique is also sensitive to (1) fatigue damage and (2) a localized stress corrosion crack. A secondary objective is to adapt the DAE experimental setup to perform measurements in smaller specimens (thickness of few cm). Several samples (intact aluminium, fatigued aluminium and steel with a stress corrosion crack) were investigated. Using signal processing not normally applied to DAE, we are able to measure the nonlinear elastic response of intact aluminium, distinguish the intact from the fatigued aluminium sample and localize different nonlinear features in the stress corrosion cracked steel sample.

**Keywords** Nonlinear acoustics · Dynamic acousto-elasticity · Micro-damage · Stress corrosion crack · Fatigue damage · Polycrystalline metals

## 1 Introduction

This research relates to important questions such as, “How can we prevent dam failure, plane crash or radioactive leakage from a nuclear power plant?” An essential part of the strategy to prevent such disasters requires the development of more accurate and sensitive structural material evaluation techniques. As it is not possible to perform destructive tests on the materials in situ, the development of effective non-destructive testing (NDT) techniques is essential. Indeed, it is fundamental to detect as early as possible initiation of a fracture that could jeopardize the operation of a nuclear power plant. Among the new emerging techniques, nonlinear acoustic techniques are very promising [1–4]. They allow one to measure the nonlinear elastic response of a medium to the passage of high-amplitude acoustic/elastic waves. This response depends on the presence of micro-defects or soft inhomogeneity (microcracks, dislocations, grain contact, delamination, etc.) that act as classical and/or non-classical nonlinear sources affecting the overall level of the material’s nonlinearity [5, 6]. The nonlinearity at the interatomic scale [7] is negligible compared to that produced by the micro-defects [5]. It is manifested first by the appearance of harmonics in the acoustic response. The concept is not new. For instance Buck et al. [8] demonstrated this effect by sending an ultrasonic wave through two solids in contact. They measured the onset of harmonics whose amplitudes were directly related to the excitation amplitude and the quality of contact between the two solids. The following year, they demonstrated that the increase in the second harmonic

---

S. Hauptert (✉)  
Laboratoire d’imagerie paramétrique, CNRS UMR 7623,  
UPMC Paris 6, 15 rue de l’école de médecine, 75006 Paris, France  
e-mail: sylvain.hauptert@upmc.fr

J. Rivière · B. Anderson · T. J. Ulrich · P. Johnson  
Geophysics Group MS D446, Earth and Environmental Sciences,  
Los Alamos National Laboratory, Los Alamos, NM 87545, USA

Y. Ohara  
Department of Materials Processing, Graduate School  
of Engineering, Tohoku University, 02 Aoba, Aramaki-aza,  
Aoba-ku, Sendai 980-8579, Japan

was associated with the fatigue of a piece of aluminum [9]. Thus the detection of harmonics became a first technical reference for NDT nonlinear acoustics [10–12]. Subsequently, other phenomena were discovered, such as the creation of sub-harmonic [13, 14], frequency mixing [6, 15] and frequency shifting [16, 17], leading to new nonlinear techniques, often termed “nonlinear elastic wave spectroscopy (NEWS)” [18, 19]. After two decades of investigation, these nonlinear techniques were applied in a wide range of applications, such as in civil engineering (i.e. concrete structures [20–26] and pipes [14, 27]), in aviation (i.e. composites [28–30] or metals [31]) and in biomedical [32, 33]. In parallel, other nonlinear methods, called *pump-probe*, were developed based on the interaction of two dynamic fields. One perturbs the material elasticity (*the pump*) while the other measures the change in the viscoelasticity (*the probe*) [34–37]. The dynamic acousto-elastic (DAE) [38–41] technique is one of them. It’s an extension of the well-known quasi-static acousto-elastic (SAE) technique [42, 43] considered to be the most precise and sensitive technique for the evaluation of the third order elastic constants in isotropic solids [7, 43]. Compared to SAE, DAE involves low strain level ( $10^{-8}$ – $10^{-5}$ ), higher strain rate (e.g. several kHz), both tension and compression stresses and does not require the use of a mechanical testing machine, which makes this technique suitable for *in-situ* measurements. Compared to NEWS techniques, DAE is the only technique that directly shows nonlinear behavior as it evolves over an entire dynamic strain cycle (i.e. during tension and compression), such as hysteresis. DAE has been used successfully so far for bone micro-damage monitoring [44–47] and nonlinear elastic investigation of rock [38–40, 48].

The main objective of the paper is to evaluate whether the DAE technique is also sensitive to (1) non-localized fatigue damage and (2) localized stress corrosion cracking in metallic specimens. A secondary objective is to adapt the DAE experimental setup to perform measurements in very small specimens (thickness of few cm).

## 2 Materials and Methods

### 2.1 Specimens and Damage Protocol

Non-localized fatigue damage and localized stress corrosion cracking (SCC) were investigated in two different sets of metallic specimens.

For the fatigue damage protocol, two AU4G aluminum bars (50 mm ( $L$ )  $\times$  4 mm ( $b$ )  $\times$  2 mm ( $d$ )) were machined from the same 2 mm thick aluminum plate. One aluminum specimen was fatigued while the other aluminum specimen was kept intact to serve as control. Fatigue damage was induced within the elastic regime by cyclic four-point

bending at 2 Hz under load-control between  $-30$  and  $-170$  N (corresponding to maximal strain of 6,000  $\mu\epsilon$  at the mid-span) using a hydraulic testing machine (Instron 8501, High Wycombe, England) with a 1 kN loading cell (accuracy 0.5 %) and an internal displacement transducer (accuracy 1 %). The fatigue test is stopped after 10,000 cycles when a slight bending is observed, meaning that permanent damage occurred. Therefore, the cyclic stress is suspected to increase the dislocation density and/or to initiate fatigue cracking at some point on the external surface [49].

For the localized stress corrosion cracking (SCC) investigation, one thin steel square specimen (23.5 mm ( $L$ )  $\times$  23.5 mm ( $b$ )  $\times$  2.4 mm ( $d$ )) was machined from a large stainless steel bar specimen. This bar contained a deep crack that was propagated from a notch by a three-point bending toughness test with a stress intensity factor between  $K_{max} = 28$  Mpa $\sqrt{m}$  and  $K_{min} = 0.6$  Mpa $\sqrt{m}$ . SCC was initiated at the crack tip [50]. A corrosive environment involving a solution of 30 wt% MgCl<sub>2</sub> at 90 °C, and a nominal bending stress of 124 Mpa was applied for 650 h. The characterization of the deep crack and the SCC was accomplished on a three-dimensional (3D) X-ray micro-computed ( $\mu$ CT) tomography volume, acquired with a non-commercial desktop  $\mu$ CT device. The isotropic voxel resolution is 21  $\mu$ m.

### 2.2 DAE Setup and Measurement Protocol

#### 2.2.1 Experimental Setup

The DAE, first proposed by Renaud et al. [41] to monitor bone microdamage accumulation in immersion [44–46], has been adapted to measure materials in a dry condition with transducers directly in contact with the sample [38]. The technique consists of broadcasting a high frequency (HF) wave, from an ultrasonic (US) transducer source (HF source) to an ultrasonic transducer receiver (HF receiver), to probe the elastic state modulated in the sample by a low frequency (LF) piezoelectric disk source (PZT-5A, APC International, Mackeyville, PA, USA) [38]. For most nonlinear materials, the typical acousto-elasticity effect results in an increasing (decreasing) of the elastic modulus when the sample is under compression (tension). Experimentally, the modulus variation is evaluated by measuring the time of flight (TOF) variation, both parameters being proportional [38]. One can also observe a variation of the attenuation [48].

The LF strain field is generated by a large piezoelectric disk attached to a backload and glued with cyanoacrylate to the bottom of each sample (Fig. 1). The LF wave is monitored by a small and light piezoelectric disk placed on the top of each sample (Fig. 1). The typical frequency  $f_{LF}$  used for the LF strain field is 29 kHz for the aluminum bar specimens and 49 kHz for the steel square specimen. Both frequencies correspond to the first compressional mode in forced-mass driven

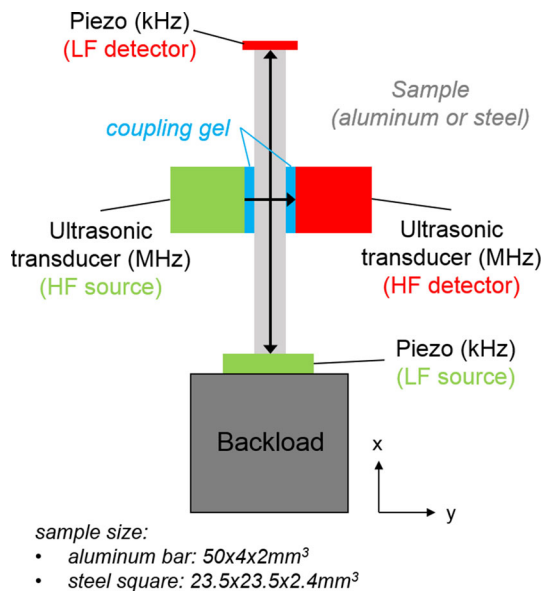


**Fig. 1** Experimental setup for both experiments

boundary conditions (the fixed-free boundary condition cannot be reached as the mass of the small piezoelectric sensor is not negligible). However, one can approximate the wavelength ( $\lambda_{LF} \approx 4L$ ,  $\lambda_{LF} \approx 200$  mm for aluminum specimen and  $\lambda_{LF} \approx 94$  mm for steel specimen) in case of fixed-free boundary conditions.

The probe is a US pulse (typically 5 HF periods) generated and received by a pulser-receiver (5077PR, Olympus, Waltham, MA, USA). Two identical ultrasonic transducers at  $F_{HF} = 25$  MHz (Panametrics, Waltham, MA, USA) with an active beam width  $d_{us}$  of 4 mm are involved. The US pulse repetition frequency (PRF) is adapted to be incommensurate with  $f_{LF}$ , so that over time the ultrasonic broadcasts sample all phases of the LF strain field. Practically, it was chosen

a little bit less than 5 kHz, in the limit of the maximal PRF delivered by the pulser-receiver (i.e. 5 kHz).

The coupling is ensured by using ultrasonic gel between the probe and the sample. Note that a thin layer of adhesive tape is applied on the crack in the steel specimen, to keep the crack dry.

The use of dynamic strain instead of the conventional static strain implies that the LF strain field seen by the US wave has to be quasi-constant during the US propagation [39–41]. For this reason, the HF wave propagation time ( $t_{HF} = d/c \approx 0.4$   $\mu$ s, with  $c$  between 5,000 m/s for steel to 6,400 m/s for aluminum) is required to be sufficiently short compared to the LF period  $T_{LF}$  ( $t_{HF}/T_{LF} \approx 0.02 \ll 1$ ). DAE also requires a quasi-uniform LF strain field in the probed volume which corresponds to the intersection between the LF acoustic field characterized by  $\lambda_{LF}$  and the US beam width  $d_{us}$  ( $d_{us}/\lambda_{LF} \approx 0.06 \ll 1$ ,  $\lambda_{LF} \approx 0.1$ – $0.2$  m). When both requirements are met, one can assume to measure an acousto-elastic effect. Finally, several HF wavelengths ( $\lambda_{HF} = c/F_{HF} \approx 250$   $\mu$ m;  $d/\lambda_{HF} \approx 8$  cycles) should propagate along the distance  $d$  in order to be able to measure the acousto-elastic effect.

In this study, the US transducers were placed at different positions in order to probe different regions of the specimens (Fig. 2). In the case of aluminum (Fig. 2a), three regions (at 10, 25 and 35 mm from the specimen's bottom along the vertical direction (x-direction)) were investigated to determine if TOF variation (i.e. nonlinear elastic properties) depends on the location. In the case of the steel specimen (Fig. 2b), the nonlinear elastic behavior was probed every 2 mm (8 regions) along the horizontal direction (z-direction) through the macrocrack, the SCC as well as the intact region.

As the DAE technique involves the measurement of small US TOF variations synchronized with the LF wave, both US and LF signals are sampled at a very high frequency ( $F_s =$

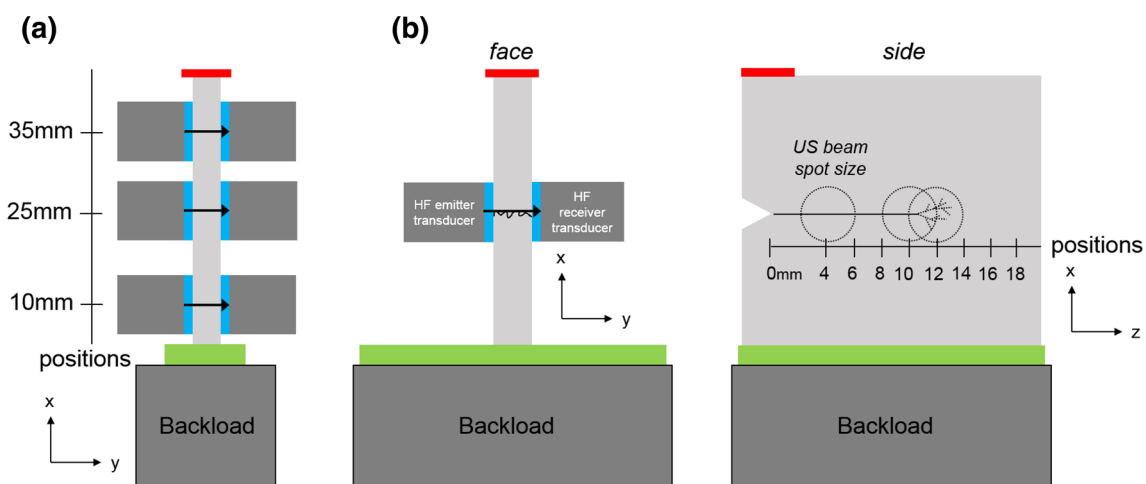


**Fig. 2** Positions of the US probe in case of aluminum specimens (a) and steel specimen (b)

1.25 GHz (PicoScope PS6403A, Picotech, Cambridgeshire, United Kingdom)) which implies to adapt the conventional DAE technique described in previous papers.

DAE experiments were performed five times with repositioning of both US transducers for all specimens and all positions. Error bars correspond to the standard error of the mean values extracted from the experimental data (see Sect. 2.2.3).

### 2.2.2 Optimization of the DAE Method

The conventional DAE method involves the acquisition of both US and LF entire signals at the same time, with a carefully synchronized trigger and clock. The reference US TOF is first extracted from US pulses acquired when the LF resonance excitation is off. The LF resonance excitation is then turn on, and US TOF measurements acquired during the resonance are compared to the reference US TOF. Times of flight are evaluated from the first arrival signal, i.e. the directly propagating wave into the sample. This procedure, used in previous studies [38–40, 48] is only possible when the entire temporal signal containing all the US pulses can be acquired at once, meaning that the acquisition card has enough on-board memory. This procedure prevents acquisitions for a long period of time (i.e. >few seconds) or at high frequency rate (i.e.  $F_s > 1$  GHz). In order to overcome this issue, we propose an optimization of the conventional DAE method where the on-board memory is no longer a critical issue.

The principle is the following. Instead of acquiring the entire temporal US and LF signals, only portions of both signals corresponding to the duration of the US wave propagation are recorded. The principal drawback of this method is that the reference and the tested US pulses are not perfectly synchronized due to jitter in the acquisition card (typically less than 1 ns, corresponding to a fraction of the sampling period). This is an important issue for weak nonlinear materials such as metals, as the TOF variation is expected to be rather small (typically less than 1 ns). Therefore the variation can be completely masked by the jitter. Note that it also induces an asynchronism between US and LF signals, however, this is not a critical issue since the LF pressure amplitude can be considered constant over few ns (i.e. the jitter duration).

In the case of a low attenuating material such as metals, the above mentioned problem can be overcome as the pulse can propagate at least twice along the same path before vanishing. Thereby, the first arrival signal (path 1 in Fig. 3) is set as the reference. This signal is compared with the second arrival signal (path 2 in Fig. 3) which is delayed or accelerated during the additional back and forth propagation in the specimen. Both pulses are acquired with the same trigger and therefore no jitter interferes with the evaluation of the TOF variation.

This procedure has another advantage. It is expected to take into account variations of the reference TOF that can be

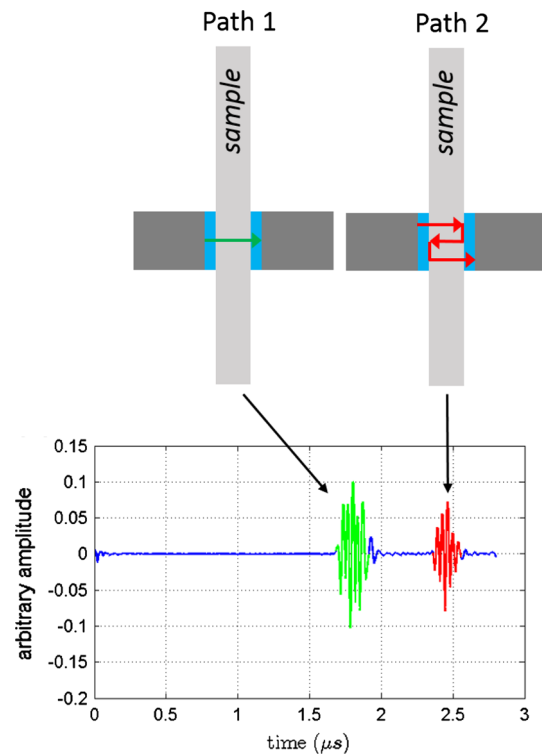


**Fig. 3** The 1st arrival signal (green) corresponds to the direct path (Path 1) while the 2nd arrival signal (red) corresponds to the back and forth propagation path (Path 2) (Color figure online)

due to environmental factors (i.e. temperature, humidity and pressure) [51], conditioning and long-time relaxation effects [39, 40, 52–54]. However, the TOF measurement is sensitive to density and thickness variation due to Poisson effect during the LF resonance. It is also sensitive to a relative change of the specimen position between the two US probes due to a slight lateral movement (i.e. bending). A rapid evaluation of these effects shows that density and thickness variations compensate each other and represents at most a TOF variation of 1 ps. An equivalent TOF variation is also expected for a lateral displacement of 10 nm [40] when the US wave travels three times through the specimen’s thickness.

### 2.2.3 Signal Processing

The signal processing used to extract the TOF variation is extensively explained in previous papers [39, 40]. Briefly, the TOF shift  $\tau$  between the reference US pulse  $s_{ref}(t)$  (i.e. the first arrival signal, path 1) and the  $j$ th US pulse  $s_j(t)$  (i.e. the second arrival signal, path 2) is calculated by cross-correlation with and without the LF strain field:

$$X_{corr}(\tau, j) = \int_0^{\infty} s_{ref}(t)s_j(t - \tau)dt \tag{1}$$

In order to extract the most accurate TOF shift  $\tau_{max}$ , corresponding to the position of the maximum cross-correlation function peak  $X_{corr}(\tau_{max})$ , the peak is interpolated by a second order polynomial function [55]. As we can assume that the TOF shift due to the Poisson effect and density modulations are negligible compared to the TOF shift due to elastic modulations, one can convert the TOF variation into a speed of sound (SOS) variation for each US pulse using [39,40]:

$$\frac{\Delta c}{c}(j) = -\frac{\tau_{max}(j)}{TOF_{ref}} \tag{2}$$

where  $c$  is the material speed of sound ( $c = 5,000$  m/s for steel and  $c = 6,400$  m/s for aluminum),  $TOF_{ref}$  is the duration of the US pulse propagating back and forth in the sample without the LF strain field.

Finally, for each US pulse  $j$ , the SOS variation  $\frac{\Delta c}{c}(j)$  can be associated with the corresponding local strain level  $\varepsilon(h, j)$  extracted from the LF strain signal at the position  $x = h$ . Then, for each position, the DAE experiment gives two synchronized and time-dependent vectors, the SOS variation and its associated local strain level. After removing the DC offset, both vectors,  $\frac{\Delta c}{c}(t)$  and  $\varepsilon(h,t)$ , can be expressed as a sum of orthonormal sine and cosine functions at given frequencies  $nw$  (where  $w = 2\pi f_{LF}$  is the LF resonance pulsation of each sample). This is performed by the means of a projection procedure and the result of the projection is denoted by the subscript  $p$  [40]:

$$\varepsilon(h, t) \approx \varepsilon(h, t)_p = \sum_{n=1}^N A_n \sin(nwt) + \sum_{n=1}^N B_n \cos(nwt) \tag{3a}$$

$$\frac{\Delta c}{c}(t) \approx \frac{\Delta c}{c}_p(t) = \sum_{n=1}^N C_n \sin(nwt) + \sum_{n=1}^N D_n \cos(nwt) \tag{3b}$$

where the coefficients  $A_n$  ( $B_n$ ) (i.e.  $C_n$  ( $D_n$ )) weigh the signal's portion in phase (out of phase) with the fundamental frequency  $w$ . Note that the phase of both vectors ( $\varepsilon(h,t)$  and  $\frac{\Delta c}{c}(t)$ ) must be adjusted beforehand such that,  $\varepsilon(h,t)$  is in phase (i.e.  $A_1 \neq 0$ ;  $B_1 \approx 0$ ) with  $w$ .  $N$  depends on the harmonic content of the signal. In this study,  $N$  is fixed to 3. The higher the coefficient  $D_n$ , the more hysteretic is the relationship between SOS variation and local strain level.  $A_1$  (i.e.  $B_1$ ) controls the amount of signal that evolves with  $w$  (linear part), whereas,  $A_2$  (i.e.  $B_2$ ) and  $A_3$  (i.e.  $B_3$ ) control the amount of signal that evolves with  $2w$  (quadratic part) and  $3w$  (cubic part), respectively. As opposed to a classic FFT analysis, this method allows the extraction of the harmonic content from a noisy and/or undersampled signal (the signal is sampled at the PRF).

Amplitudes found from this projection procedure will help us extract nonlinear parameters from the complex signatures obtained experimentally. For instance, we define a parameter  $\beta$  as the ratio between the magnitude of the SOS variation  $\left. \frac{\Delta c}{c} \right|_{1w}$  evolving with  $w$ , and the magnitude of the strain  $\Delta\varepsilon$  over one period [39,40]:

$$\left. \frac{\Delta c}{c} \right|_{1w} = \sqrt{C_1^2 + D_1^2} \tag{4}$$

$$\Delta\varepsilon = \varepsilon_{max} - \varepsilon_{min} \tag{5}$$

$$\beta = 2 * \frac{\left. \frac{\Delta c}{c} \right|_{1w}}{\Delta\varepsilon} \tag{6}$$

where  $\varepsilon_{max}$  and  $\varepsilon_{min}$  are the maximal and minimal strain excursion over one period respectively. This parameter is equivalent to the quadratic nonlinear elastic parameter [56] if no hysteresis is present in the nonlinear signature. Note that Eq. 6 gives the absolute value of  $\beta$ , as the sign is not taken into account when calculating  $\left. \frac{\Delta c}{c} \right|_{1w}$ . The parameter is comparable with the one obtained by the common method based on the 2nd harmonic generation [57].

We define a second parameter  $\alpha$  which depends on the magnitude of the SOS variation at null strain  $\left. \frac{\Delta c}{c} \right|_{\varepsilon=0}$  and the magnitude of the strain  $\Delta\varepsilon$  over one period [39,40]:

$$\alpha = 2 * \frac{\left. \frac{\Delta c}{c} \right|_{\varepsilon=0}}{\Delta\varepsilon} \tag{7}$$

This second parameter is similar to the hysteretic elastic nonlinear parameter if the nonlinear signature is a bowtie shape [56].

### 2.2.4 Low Frequency Strain Field Investigation

The strain level is required to compare the nonlinear behavior between specimens and regions for the same specimen. The strain level is expected to be different throughout the sample as the low frequency strain field of the specimens is not homogeneous. In previous experiments [38–40,48], the strain field was estimated analytically based on the assumption that the boundary condition of the 1st resonant mode was fixed-free. In this paper, the forced-mass driven boundary condition prevents analytical estimation of the local strain. The local strain levels of the probed regions were then investigated experimentally by measuring the axial (x-direction) particle velocity  $v(x)$  with a fiber-optic differential laser vibrometer [58] (Polytec OFV 552, Irvine, CA, USA) when the specimens were excited at their 1st compressional mode (x-direction). The grid step of the laser was 1 mm. The velocity measurements were performed on the same side as the US emitter transducers positions. The local strain level  $\varepsilon(x)$  was estimated by calculating the spatial difference of the particle velocity:

$$\varepsilon(x) = \frac{1}{c} \frac{\Delta v(x)}{\Delta x} \tag{8}$$



where  $c$  is material speed of sound ( $c = 5,000$  m/s for steel and  $c = 6,400$  m/s for aluminum) and  $x$  is the axial coordinate of the particle.

The global strain signal (time signal) measured with the PZT glued on the top of each specimen is then normalized to the local strain level. There was no need to adjust the phase of the global signal as global and local signals were found to be in-phase at each probe location.

### 3 Results

#### 3.1 Optimization of the DAE Method

The optimization of the DAE method was validated on the intact aluminum specimen. The results obtained with the new DAE procedure (i.e. the reference US pulse is the first arrival signal while the tested US pulse is the second arrival signal) and with the conventional procedure (i.e. the reference and tested pulses are acquired separately, both being the first arrival signal) are shown in Fig. 4. No variation of the TOF values is observed when the strain field is applied with the conventional method while variations are clearly visible with the new procedure. Moreover, the TOF sensitivity assessed when no strain field is applied (red and green portions on Fig. 4a, b) is one order of magnitude higher (i.e. sensitivity is 0.01 ns with new procedure while it is 0.1 ns for the conventional procedure). Interestingly, one can notice a slight TOF decay at the beginning of the measurement while no strain field is applied (red portion on Fig. 4a) confirming a drawback of the conventional method: reference TOF which should remain constant throughout the experiment can change. This drawback is overcome with the new method as no TOF variation is noticeable for the same time period (red portion on Fig. 4b).

When comparing the SOS variation for different LF strain levels (Fig. 4c, d), one can notice that the nonlinear signature is only noticeable with the new method (Fig. 4d). This confirms that high TOF sensitivity is required to be able to extract the weak nonlinear signature of the aluminum specimen. The maximal speed of sound variation for the intact aluminum is 0.01% for a strain level of  $10^{-5}$ . Moreover, it is also possible with the new procedure to observe a different nonlinear behavior when the strain increases or decreases as well as a small hysteresis.

#### 3.2 Comparison Between Intact and Fatigued Aluminum Specimens

The maximal strain achieved at position {10, 25, 35 mm} is found to be {1.07, 0.77, 0.42}  $\mu\epsilon$  for the intact specimen and {1.41, 0.84, 1.05,}  $\mu\epsilon$  for the damaged specimen. Typical TOF modulation (i.e. SOS variation) range from 0.05 ns

(i.e. 0.01%) for measurements performed at 35 mm (i.e. where the strain level is the lowest) in case of intact aluminum specimen, to about 0.15 ns (i.e. 0.03%) for the measurement performed at the center (i.e. at 25 mm) of the damaged specimen.

The intact aluminum specimen results in similar raw curves (similar slope and hysteresis) for all the measurement positions, while the fatigued aluminum specimen displays different curves (Fig. 5a–c). Hysteresis and slopes are higher for the damaged aluminum specimen than the intact aluminum. Only the fatigued aluminum specimen shows an increase followed by a decrease of the slope. Its hysteresis increases gradually from bottom (i.e. where the strain level is the highest) to top (i.e. where the strain level is the lowest) of the specimen. In order to compare intra and inter specimen trends, projection procedure analysis was performed on each raw curve and the fitted curves are displayed in Fig. 5b–d. Then, nonlinear  $\beta$  and  $\alpha$  parameters are calculated following Eqs. 6 and 7, respectively. For the intact aluminum specimen, the absolute  $\beta$  parameter {21.7  $\pm$  2.3, 22.7  $\pm$  6.7, 26.5  $\pm$  7.9} is almost constant for each position while the absolute  $\beta$  parameter for the fatigued specimen {32.8  $\pm$  11.6, 74.6  $\pm$  14.7, 53.2  $\pm$  2.7} is not constant along the specimen. The maximum  $\beta$  value is measured in the center of the damaged specimen (74.6  $\pm$  14.7) where the maximum damage (mainly dislocations and microcracks) is expected to occur during the four-point bending fatigue test (Fig. 6).

Finally, no significant  $\alpha$  value was measured for both aluminum specimens as the variability of the SOS variation at null strain  $\left. \frac{\Delta c}{c} \right|_{\epsilon=0}$  required to estimate  $\alpha$  was too high.

#### 3.3 Steel with Crack and Stress Corrosion Crack (SCC)

The maximal strain achieved along the crack in the steel specimen {4, 6, 8, 10, 12, 14, 16, 18} mm is found to be {4.4, 3.9, 4.4, 2.1, 1.5, 2.5, 2.2, 2.3}  $\mu\epsilon$  (see Fig. 7), corresponding to a displacement range between 16 and 50 nm. Typical TOF modulations (i.e. SOS variation) range from 0.03 ns (i.e. 0.002%) for the measurement performed at position 18 mm (i.e. where there is no crack nor SCC) to about 0.15 ns (i.e. 0.01%) for the measurement performed at the crack tip encompassing the SCC area (i.e. at 12 mm).

The projection analysis in Fig. 8 shows that the maximum acousto-elastic effect (higher TOF modulation and largest hysteresis) is produced near the crack tip (i.e. probe position = 10 mm) as well as in the SCC area (i.e. probe position = 12 mm).

The nonlinear parameters, the classical  $\beta$  and the non-classical  $\alpha$ , are calculated following Eqs. 6 and 7, respectively, and results are presented in Fig. 7. The  $\beta$  values are lower outside the crack tip and the SCC area, with an average value of 15.8  $\pm$  6.0 while  $\beta$  is 62.4  $\pm$  5.2 in the crack tip region and  $\beta$  is 116.0  $\pm$  27.5 in the SCC region. The trend is

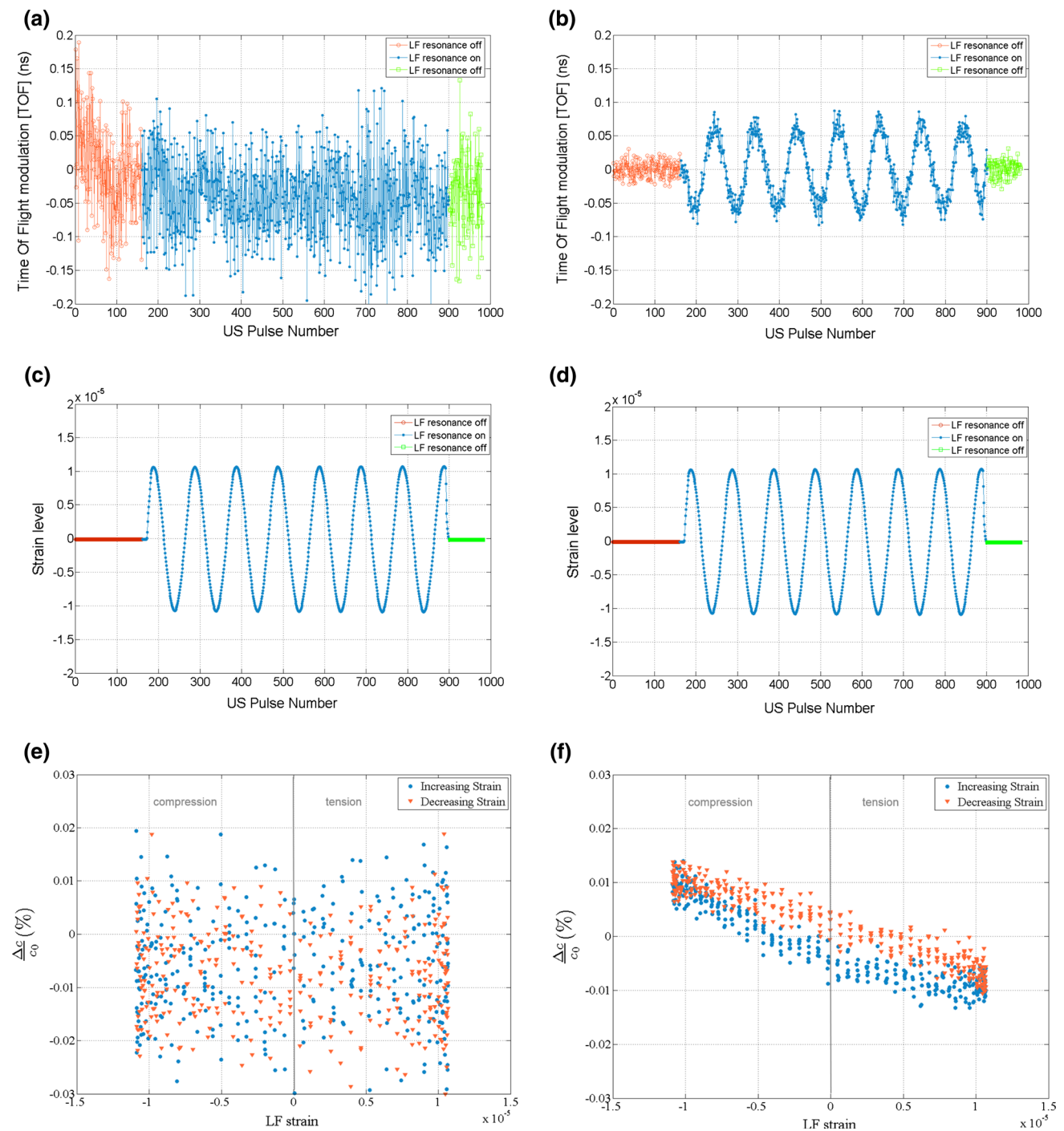


**Fig. 4** Comparison between conventional (a, c, e) and optimized (b, d, f) DAE. a, b Time of flight variation; c, d LF strain; e, f relative velocity change versus LF strain. The measurements were performed at position 10 mm on intact aluminum specimen

different for the  $\alpha$  parameter. Its value is almost null before the crack tip (between 4 and 8 mm), in the SCC region (at 12 mm) and in the intact region (between 14 and 18 mm). At the crack tip, the  $\alpha$  value is negative with a large standard deviation ( $\alpha = -16.7 \pm 20.9$ ). Such a large deviation of  $\alpha$  ( $\pm 20.3$ ) is also visible in the SCC region.

The crack thickness is roughly 200  $\mu\text{m}$  before the crack tip (Fig. 8). The gap between both lips of the crack is not constant through the specimen thickness. In the SCC region, due to the resolution of the  $\mu\text{CT}$  (i.e. 20  $\mu\text{m}$ ), one can only detect crack thicknesses larger than 20  $\mu\text{m}$ . This does not mean that smaller cracks are not present in this region.

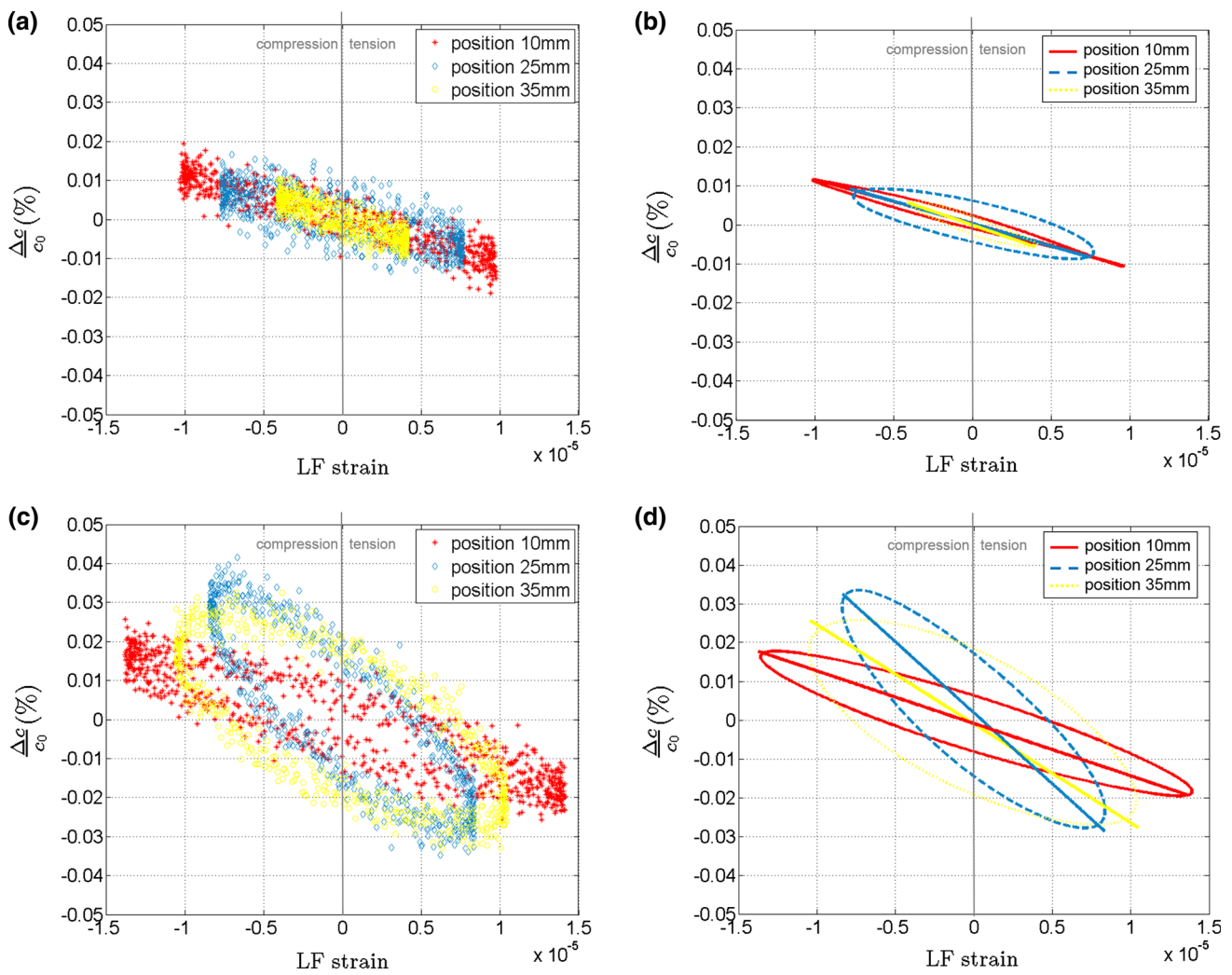


**Fig. 5** Raw DAE data measured at position { 10, 25, 35 } mm of the intact (a) and the fatigued (c) aluminum; and after reconstruction by projections method (intact (b) and fatigued (d)). The slope of the linear fits corresponds to  $\beta$  calculated following Eq. 7

### 4 Discussion

This study represents the first attempt to perform DAE in small metallic specimens (thickness of few cm). As it requires a high frequency ultrasonic probe (>20 MHz), the conventional DAE method was optimized and validated in an intact aluminum specimen.

#### 4.1 Optimized DAE Method

The results showed that a nonlinear elastic signature is solely measurable with the optimized method with this experimental setup (Fig. 4). Indeed, the sensitivity of the optimized DAE method was found to be one order of magnitude higher (i.e. sensitivity is 0.01 ns with the optimized procedure while it is 0.1 ns for the conventional procedure). This allows the detection of small TOF variations required to characterize nonlinear elastic behavior of weak nonlinear materials.

Interestingly, as the reference US pulse is measured before each tested US pulse, the new DAE method is expected to take into account small variations of the reference TOF throughout the experiment. These variations can be due to environmental factors (i.e temperature, humidity and pressure) [51], conditioning and long-time relaxation effects [39,40,52–54]. Thereby, one can also expect to dissociate fast from slow non-linear elastic dynamics in TOF variation in materials (e.g. rocks) where both phenomenon are very noticeable [40,48].

#### 4.2 Distinction Between Intact and Fatigued Damage

The optimized DAE was then applied for the first time to monitor two different kinds of damage in small metallic samples: diffuse fatigue damage and localized stress corrosion cracking. The results show that optimized DAE method is able to distinguish between intact and fatigued damaged



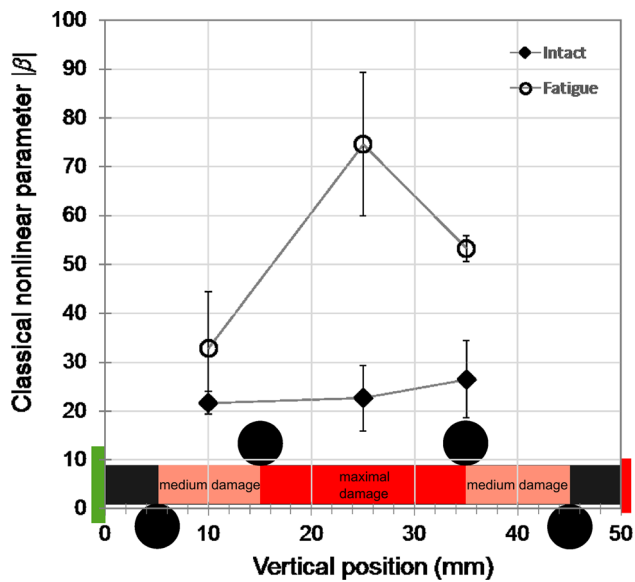


**Fig. 6** Classical nonlinear parameter  $|\beta|$  variation depending on the vertical position along the aluminum bar specimens (intact and fatigued)

aluminum specimens and to localize the crack tip and the SCC region in the steel specimen.

The classical nonlinear parameter  $\beta$  extracted from DAE data is doubled for the fatigue aluminum specimen compared to the intact specimen. Moreover, the highest  $\beta$  value is obtained at the position 25 mm (i.e. the specimen center), where the fatigue damage is expected to be the most severe after a four-point bending fatigue test [49].

The intact aluminum specimen exhibits an average  $\beta$  value that is larger than the value generally found in the literature for single aluminum crystal [38,57,59]. However, one has to notice that the specimen is not a single aluminum crystal but an aluminum alloy (AU4G). AU4G aluminum is a polycrystalline material, composed of a multitude of grains separated by grain boundaries. Grains may also contain dislocations due to the preparation process (cutting). Both grain boundaries and dislocations are known to produce nonlinear elastic behavior in materials [60]. This may explain the large  $\beta$  value measured in an aluminum alloy (AU4G), which is of the same order of magnitude as other metallic alloys (steel in

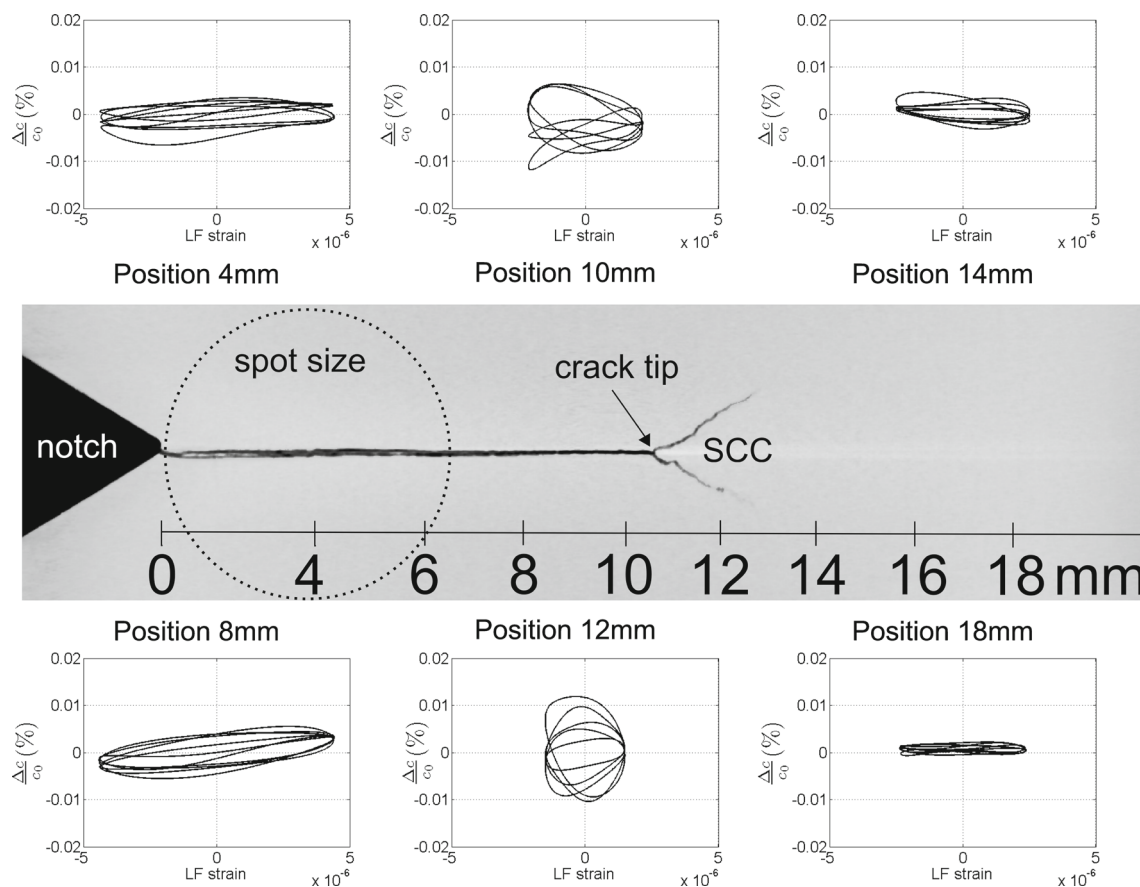


**Fig. 7** Superposition of all the five DAE reconstructed signatures measured along the crack (z-direction) for positions {4, 8, 10, 12, 14, 18} mm. 2D transverse image extracted from the 3D  $\mu$ CT volume

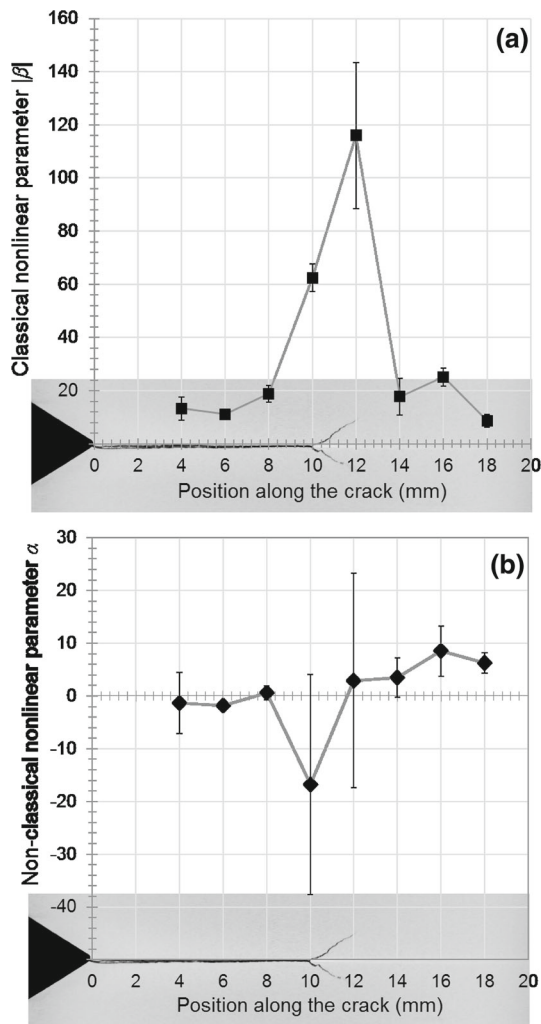


**Fig. 8** Variation of the classical and non-classical nonlinear parameters  $|\beta|$  (a) and  $\alpha$  (b) along the crack (z-direction)

this study or Inconel  $\beta = 21.4$  [12]). Note that the  $\beta$  parameter calculated in this study is the absolute value. The sign of the  $\beta$  value corresponds somehow to the slope of the linear fit of the nonlinear DAE signature in Fig. 5. The sign of  $\beta$  was found to be negative, as expected for most metallic materials [42]. From Eq. 6, a negative  $\beta$  means that the elastic modulus (i.e. the speed of sound) increases when the strain is negative (i.e. compression) and decreases when the strain is positive (i.e. tension).

Aluminum alloy (AU4G) is known to exhibit weak non-classical nonlinear elastic behavior as other metallic materials [51]. However, in this study, it was not possible to assess the non-classical nonlinear parameter  $\alpha$  in both intact and damage aluminum specimens by DAE. This was partly due to the large variability of the SOS variation at null strain  $(\frac{\Delta c}{c})_{\epsilon=0}$ . The optimized DAE method is maybe not yet as sensitive as the optimized Nonlinear Resonant Ultrasound Spectroscopy (NRUS) method developed by Hauptert et al.

[51], to be able to detect and measure weak non-classical nonlinear elastic behavior.

### 4.3 Localization of Stress Corrosion Crack (SCC)

The steel specimen with localized damage exhibits the largest  $\beta$  value at the crack tip and in the SCC region, with a  $\beta$  value between 5 and 10 times higher than outside of the crack region. This result indicates that DAE would be a good candidate to carefully investigate the nonlinear elastic behavior of SCC.

Note the large error bar for  $\beta$  in the SCC region. This could be due to the repositioning. Indeed, after each repositioning, the HF US transducer (i.e. small wavelength:  $\lambda_{us} \approx 250 \mu\text{m}$ ) might not probe exactly the same nonlinear features in the SCC region. Therefore, the relative position between the HF US probe and the nonlinear sources is crucial and confirms the high sensitivity of DAE technique to SCC.

Outside of the crack region (position 14, 16 and 18mm), the  $\beta$  value was found to be close to the  $\beta$  value measured in the intact aluminum alloy specimen, and of the same order of magnitude as other metallic alloys [12]. This suggests that the  $\beta$  value in this region might be representative of the classical nonlinear parameter of an intact steel specimen.

In the open crack region (position 4, 6 and 8mm), the classical nonlinear elasticity is similar to that found outside of the crack region, meaning that the open crack does not act as a nonlinear source. This may be explained by an insufficient displacement (i.e. less than  $0.1 \mu\text{m}$ ) to close the large gap (around  $200 \mu\text{m}$ ) between the crack lips. Thus, the nonlinear mechanism, so-called clapping effect, induced by the alternative contact of crack lips, cannot be generated.

The sign of  $\beta$  was found to be negative outside of the crack region, as found for aluminum specimens, while for the steel sample, the sign is positive in the open crack region as well as at the crack tip and in the SCC region. The nature of damage could explain this opposite behavior. For example, a positive  $\beta$  value was found for cracked Pyrex [41] while intact Pyrex exhibited a negative value.

Interestingly, non-classical nonlinear behavior was measured at the crack tip and in the SCC region. Contrary to that found for the  $\beta$  value, the  $\alpha$  value is larger at the crack tip than in the SCC region. For both positions, the error bars are huge. The same explanation for the  $\beta$  value observations is proposed.

### 4.4 Hysteresis in the Nonlinear Signature

The hysteresis is present in the nonlinear signature of all the specimens. Its size increases when the  $\beta$  value increases. An hysteresis is expected in materials with non-classical nonlinear elastic behavior while classical nonlinear elasticity due to atomic anharmonicity does not produce hysteresis [61].

However, in the case of a non-classical nonlinear material, the hysteresis is expected to be bow tie-shape like, not ellipsoid-shape like. This was shown experimentally in numerous rocks samples [40,48] and can be predicted by the quadratic hysteretic model [61]. This is the first time that an ellipsoid-shape is observed in a weak nonlinear material. This behavior is due to a delay (phase-shift) between the strain signal and the TOF modulation signal. As no phase-shift was observed between the local strains, as well as between the local and the global strain measured at the piezo-ceramics receiver, the phase-shift can only be explained by the presence of an out-of-phase signal ( $D_n$ ) in the TOF modulation signal. Thereby, the hysteresis may not be due to a phase-shift between local strains, but rather this suggests that the phase-shift comes from the stress. As the stress reflects not only the elastic behavior of the material but also its viscosity, one can suggest that DAE is sensitive to local variations of the viscosity [62,63], that could be for instance generated by friction inside the microcracks. Further experiments need to be carried out to explain the origin of the ellipsoid-shape and bow tie-shape hysteresis as well as its link with micro-damage characteristics.

## 5 Conclusion

This study represents the first attempt to perform DAE measurements in small metallic specimens (thickness of few cm). An optimized DAE method was proposed and validated in an intact, small aluminum specimen. The sensitivity of the new method was found to be one order of magnitude higher than the conventional method with the same experimental setup. This was sufficient for detection of the small TOF variations required to characterize the nonlinear elastic behavior of weak nonlinear materials, such as metals.

The optimized DAE method was then applied for the first time to monitor two different kinds of damage: diffuse fatigue damage and localized SCC. The results show that DAE is able to discriminate aluminum samples with fatigue damage from intact, moreover, the largest nonlinear behavior was found to match the zone where the fatigue damage is expected to be the most severe. It was also shown that DAE is sensitive to SCC and was able to distinguish the SCC from the open crack and the crack tip. Both types of damage lead to an increase in the quadratic classical nonlinear behavior (i.e.  $\beta$  value) as well as the hysteresis of the nonlinear DAE signature. Further experiments need to be done in order to explain the origin of this hysteresis and adapt the nonlinear models. As the experiment was conducted only on a few specimens, results have to be confirmed with more samples, monitoring the nonlinear DAE signature as the damage (fatigue damage, single microcrack or SCC) is increased and correlating the nonlinear parameters (e.g.  $\alpha$ ,  $\beta$ , etc.) with the damage

features (e.g. dislocations density, total grain boundaries area, microcracks length and density, etc.).

Although the DAE technique is not easily applicable for in-situ measurements, it has been demonstrated in this study that this technique is a promising tool to investigate the nonlinear elastic behavior of a large variety of localized damage (e.g. dislocations, stress corrosion cracks, microcracks, close/open cracks, bonding, delaminations, etc.).

**Acknowledgments** This work was supported in part by the U.S. Dept. of Energy, Nuclear Energy Fuel Cycle Research and Development program under the Used Fuel Disposition campaign as part of the storage demonstration and experimentation efforts and by Institutional Support (LDRD) at Los Alamos.

## References

- Zheng, Y.P., Maev, R.G., Solodov, I.Y.: Nonlinear acoustic applications for material characterization: a review. *Can. J. Phys.* **77**, 927–967 (1999)
- Ostrovsky, L.A., Johnson, P.A.: Dynamic nonlinear elasticity in geomaterials. *Riv. Del Nuovo Cimento*. **24**, 1–46 (2001)
- Jhang, K.Y.: Nonlinear ultrasonic techniques for nondestructive assessment of micro damage in material: a review. *Int. J. Precis. Eng. Manuf.* **10**, 123–135 (2009)
- Rudenko, O.V.: Giant nonlinearities in structurally inhomogeneous media and the fundamentals of nonlinear acoustic diagnostic techniques. *Phys.-Usp.* **49**, 69 (2006)
- Guyer, R.A., Johnson, P.A.: *Nonlinear Mesoscopic Elasticity: The Complex Behaviour of Rocks, Soil, Concrete*. Wiley, New York (2009)
- Van den Abeele, K., Johnson, P.A., Sutin, A.: Nonlinear elastic wave spectroscopy (NEWS) techniques to discern material damage, part I: nonlinear wave modulation spectroscopy (NWMS). *Res. Nondestruct. Eval.* **12**, 17–30 (2000)
- Landau, L., Lifshitz, E.: *Theory of Elasticity*. Pergamon, Oxford (1986)
- Buck, O., Morris, W.L.: Acoustic harmonic-generation at unbonded interfaces and fatigue cracks. *J. Acoust. Soc. Am.* **64**, S33–S33 (1978)
- Buck, O., Morris, W.L., Inman, R.V.: Acoustic harmonic-generation due to fatigue damage in high-strength aluminum. *J. Metals* **31**, F5 (1979)
- Cantrell, J., Yost, W.: Nonlinear ultrasonic characterization of fatigue microstructures. *Int. J. Fatigue* **23**, 487–490 (2001)
- Frouin, J., Sathish, S., Matikas, T.E., Na, J.K.: Ultrasonic linear and nonlinear behavior of fatigued Ti–6Al–4V. *J. Mater. Res.* **14**, 1295–1298 (1999)
- Kim, J.Y., Jacobs, L.J., Qu, J., Littles, J.W.: Experimental characterization of fatigue damage in a nickel-base superalloy using nonlinear ultrasonic waves. *J. Acoust. Soc. Am.* **120**, 1266 (2006)
- Solodov, I., Wackerl, J., Pfeiderer, K., Busse, G.: Nonlinear self-modulation and subharmonic acoustic spectroscopy for damage detection and location. *Appl. Phys. Lett.* **84**, 5386 (2004)
- Ohara, Y., Mihara, T., Sasaki, R., Ogata, T., Yamamoto, S., Kishimoto, Y., Yamanaka, K.: Imaging of closed cracks using nonlinear response of elastic waves at subharmonic frequency. *Appl. Phys. Lett.* **90**, 011902 (2007)
- Donskoy, D., Sutin, A., Ekimov, A.: Nonlinear acoustic interaction on contact interfaces and its use for nondestructive testing. *NDT & E Int.* **34**, 231–238 (2001)

16. Van den Abeele, K., Carmeliet, J., Ten Cate, J.A., Johnson, P.A.: Nonlinear elastic wave spectroscopy (NEWS) techniques to discern material damage, part II: single-mode nonlinear resonance acoustic spectroscopy. *Res. Nondestruct. Eval.* **12**, 31–42 (2000)
17. Nazarov, V.E., Ostrovsky, L.A., Soustova, I.A., Sutin, A.M.: Nonlinear acoustics of micro-inhomogeneous media. *Phys. Earth. Planet. Inter.* **50**, 65–73 (1988)
18. Guyer, R.A., Johnson, P.A.: Nonlinear mesoscopic elasticity: evidence for a new class of materials. *Phys. Today* **52**, 30–36 (1999)
19. Johnson, P.A.: The new wave in acoustic testing. *Mater. World* **7**, 544–546 (1999)
20. Van den Abeele, K., De Visscher, J.: Damage assessment in reinforced concrete using spectral and temporal nonlinear vibration techniques. *Cem. Conc. Res.* **30**, 1453–1464 (2000)
21. Bentahar, M., El Aqra, H., El Guerjouma, R., Griffa, M., Scalerandi, M.: Hysteretic elasticity in damaged concrete: quantitative analysis of slow and fast dynamics. *Phys. Rev. B* **73**(1), 014116 (2006)
22. Zardan, J.P., Payan, C., Garnier, V., Salin, J.: Effect of the presence and size of a localized nonlinear source in concrete. *J. Acoust. Soc. Am.* **128**(1), EL38–42 (2010)
23. Payan, C., Garnier, V., Moysan, J., Johnson, P.A.: Applying nonlinear resonant ultrasound spectroscopy to improving thermal damage assessment in concrete. *J. Acoust. Soc. Am.* **121**, EL125–130 (2007)
24. Bouchaala, F., Payan, C., Garnier, V., Balaýssac, J.P.: Carbonation assessment in concrete by nonlinear ultrasound. *Cem. Concr. Res.* **41**, 557–559 (2011)
25. Antonaci, P., Bruno, C., Bocca, P., Scalerandi, M., Gliozzi, A.: Nonlinear ultrasonic evaluation of load effects on discontinuities in concrete. *Cem. Concr. Res.* **40**, 340–346 (2010)
26. Zagrai, A., Donskoy, D., Chudnovsky, A., Golovin, E.: Micro- and macroscale damage detection using the nonlinear acoustic vibro-modulation technique. *Res. Nondestruct. Eval.* **19**, 104–128 (2008)
27. Courtney, C., Drinkwater, B., Neild, S., Wilcox, P.: Factors affecting the ultrasonic intermodulation crack detection technique using bispectral analysis. *NDT & E Int.* **41**, 223–234 (2008)
28. Van den Abeele, K., Van de Velde, K., Carmeliet, J.: Inferring the degradation of pultruded composites from dynamic nonlinear resonance measurements. *Polym. Compos.* **22**, 555–567 (2001)
29. Bentahar, M., El Guerjouma, R.: Monitoring progressive damage in polymer-based composite using nonlinear dynamics and acoustic emission. *J. Acoust. Soc. Am.* **125**, EL39 (2009)
30. Van den Abeele, K., Le Bas, P., Van Damme, B., Katkowski, T.: Quantification of material nonlinearity in relation to microdamage density using nonlinear reverberation spectroscopy: Experimental and theoretical study. *J. Acoust. Soc. Am.* **126**, 963 (2009)
31. Van Damme, B., Van Den Abeele, K., Bou Matar, O.: The vibration dipole: a time reversed acoustics scheme for the experimental localisation of surface breaking cracks. *Appl. Phys. Lett.* **100**, 084103 (2012)
32. Muller, M., Mitton, D., Talmant, M., Johnson, P., Laugier, P.: Nonlinear ultrasound can detect accumulated damage in human bone. *J. Biomech.* **41**, 1062–1068 (2008)
33. Rivière, J., Hauptert, S., Laugier, P., Ulrich, T., Le Bas, P.Y., Johnson, P.A.: Time reversed elastic nonlinearity diagnostic applied to mock osseointegration monitoring applying two experimental models. *J. Acoust. Soc. Am.* **131**, 1922–1927 (2012)
34. Nazarov, V.E.: Nonlinear damping of sound by sound in metals. *Sov. Phys. Acoust.-Ussr.* **37**, 616–619 (1991)
35. Nazarov, V.E., Kolpakov, A.B., Radostin, A.V.: Amplitude dependent internal friction and generation of harmonics in granite resonator. *Acoust. Phys.* **55**, 100–107 (2009)
36. Zaitsev, V., Gusev, V., Castagnede, B.: Luxemburg-Gorky effect retooled for elastic waves: a mechanism and experimental evidence. *Phys. Rev. Lett.* **89**, 105502 (2002)
37. Westervelt, P.J.: Scattering of sound by sound. *J. Acoust. Soc. Am.* **29**, 199–203 (1957)
38. Renaud, G., Talmant, M., Callé, S., Defontaine, M., Laugier, P.: Nonlinear elastodynamics in micro-inhomogeneous solids observed by head wave based dynamic acoustoelastic testing. *J. Acoust. Soc. Am.* **130**(6), 3583–3589 (2011)
39. Renaud, G., Riviere, J., Hauptert, S., Laugier, P.: Anisotropy of dynamic acoustoelasticity in limestone, influence of conditioning, and comparison with nonlinear resonance spectroscopy. *J. Acoust. Soc. Am.* **133**, 3706–3718 (2013)
40. Rivière, J., Renaud, G., Guyer, R.A., Johnson, P.A.: Pump and probe waves in dynamic acousto-elasticity: comprehensive description and comparison with nonlinear elastic theories. *J. Appl. Phys.* **114**, 054905 (2013)
41. Renaud, G., Callé, S., Defontaine, M.: Remote dynamic acoustoelastic testing: elastic and dissipative acoustic nonlinearities measured under hydrostatic tension and compression. *Appl. Phys. Lett.* **94**, 011905 (2009)
42. Hamilton, M.F., Blackstock, D.T.: *Nonlinear acoustics*. Academic Press, San Diego (1998)
43. Winkler, K.W., Liu, X.: Measurements of third-order elastic constants in rocks. *J. Acoust. Soc. Am.* **100**, 1392 (1996)
44. Renaud, G., Calle, S., Remenieras, J.P., Defontaine, M.: Non-linear acoustic measurements to assess crack density in trabecular bone. *Int. J. Non-Linear Mech.* **43**, 194–200 (2008)
45. Moreschi, H., Calle, S., Guerard, S., Mitton, D., Renaud, G., Defontaine, M.: Monitoring of trabecular bone induced microdamage using a nonlinear wave-coupling technique. In: *Ultrasonic Symposium(IUS), IEEE International, IEEE*, 550–553 (2009)
46. Renaud, G., Calle, S., Remenieras, J.P., Defontaine, M.: Exploration of trabecular bone nonlinear elasticity using time-of-flight modulation. *IEEE Trans. Ultrason. Ferroelectri. Freq. Control.* **55**, 1497–1507 (2008)
47. Moreschi, H., Callé, S., Guerard, S., Mitton, D., Renaud, G., Defontaine, M.: Monitoring trabecular bone microdamage using a dynamic acousto-elastic testing method. *Proc. Insti. Mech. Eng. H* **225**, 1–12 (2011)
48. Renaud, G., Le Bas, P.-Y., Johnson, P.A.: Revealing highly complex elastic nonlinear (anelastic) behavior of Earth materials applying a new probe: dynamic acoustoelastic testing. *J. Geophys. Res.* **117**(B6), 1–17 (2012)
49. *Elements of Metallurgy and Engineering Alloys*. ASM International, Materials Park (2008)
50. Ohara, Y., Endo, H., Mihara, T., Yamanaka, K.: Ultrasonic measurement of closed stress corrosion crack depth using subharmonic phased array. *Jpn. J. Appl. Phys.* **48**, 07GD01 (2009)
51. Hauptert, S., Renaud, G., Riviere, J., Talmant, M., Johnson, P.A., Laugier, P.: High-accuracy acoustic detection of nonclassical component of material nonlinearity. *J. Acoust. Soc. Am.* **130**, 2654–2661 (2011)
52. Tencate, J.A.: Slow dynamics of earth materials: an experimental overview. *Pure and Appl. Geophys.* **168**(12), 2211–2219 (2011)
53. TenCate, J.A., Smith, E., Guyer, R.A.: Universal slow dynamics in granular solids. *Phys. Rev. Lett.* **85**, 1020–1023 (2000)
54. Johnson, P., Sutin, A.: Slow dynamics and anomalous nonlinear fast dynamics in diverse solids. *J. Acoust. Soc. Am.* **117**, 124–130 (2005)
55. Céspedes, I., Huang, Y., Ophir, J., Spratt, S.: Methods for estimation of subsample time delays of digitized echo signals. *Ultrason. Imaging* **17**, 142–171 (1995)
56. Van den Abeele, K., Sutin, A., Carmeliet, J., Johnson, P.A.: Microdamage diagnostics using nonlinear elastic wave spectroscopy (NEWS). *NDT & E Int.* **34**, 239–248 (2001)
57. Cantrell, J.H., Yost, W.T.: Acoustic harmonic generation from fatigue-induced dislocation dipoles. *Philos. Mag. A* **69**, 315–326 (1994)



58. Ulrich, T.J., Van Den Abeele, K., Le Bas, P.-Y., Griffa, M., Anderson, B.E., Guyer, R.A.: Three component time reversal: focusing vector components using a scalar source. *J. Appl. Phys.* **106**, 113504 (2009)
59. Sarma, V.P.N., Reddy, P.J.: Third-order elastic constants of aluminium. *Physica Status Solidi (a)*. **10**, 563–567 (1972)
60. Hikata, A., Chick, B.B., Elbaum, C.: Dislocation contribution to the second harmonic generation of ultrasonic waves. *J. Appl. Phys.* **36**, 229–236 (1965)
61. VandenAbeelee, K.E.A., Johnson, P.A., Guyer, R.A., McCall, K.R.: On the quasi-analytic treatment of hysteretic nonlinear response in elastic wave propagation. *J. Acoust. Soc. Am.* **101**, 1885–1898 (1997)
62. Trarieux, C., Callé, S., Poulin, A., Tranchant, J.-F., Moreschi, H., Defontaine, M.: Measurement of nonlinear viscoelastic properties of fluids using dynamic acoustoelastic testing. In: *IOP Conference Series: Mater. Sci. Eng.* **42**, 012026. (2012)
63. Trarieux, C., Calle, S., Moreschi, H., Poulin, A., Tranchant, J.F., Defontaine, M.: An analytical model to describe nonlinear viscoelastic properties of fluids measured by dynamic acoustoelastic testing. In: *Ultrasonic Symposium(IUS)*, IEEE, 1–4 (2012)